



Bifurcation analysis of a resistor-double inductor and double diode circuit and a comparison with a resistor-inductor-diode circuit in phase space and parametrical responses

E. Kurt^{a,*}, B. Ciylan^b, O.O. Taskan^a and H.H. Kurt^c

- a. Department of Electrical and Electronics Engineering, Faculty of Technology, Gazi University, 06500 Teknikokullar, Ankara, Turkey.
b. Department of Computer Engineering, Faculty of Technology, Gazi University, 06500 Teknikokullar, Ankara, Turkey.
c. Department of Physics, Faculty of Sciences, Gazi University, 06500 Teknikokullar, Ankara, Turkey.

Received 28 April 2013; received in revised form 31 July 2013; accepted 10 February 2014

KEYWORDS

Bifurcation;
Center manifold;
Chaos;
Resistor-inductor-
diode circuit.

Abstract. In this paper experimental and analytical explorations of an R - $2L$ - $2D$ circuit were carried out. The responses from the ordinary em RL-Diode and R - $2L$ - $2D$ circuits were characterized and compared for a wide parameter region. As a new circuit, R - $2L$ - $2D$ has an additional

inductor and a diode. The circuit had different attractors compared with the ordinary RL -Diode circuit. It was proven that the new circuit exhibited wider chaotic regions on the parameter space (i.e. input voltage, V_f , and frequency, f). Both even and odd subharmonic responses were observed following the multiple periodic doublings. The bifurcation analysis revealed the dominance of feeding frequency by means of the center manifold theory. However, periodic and chaotic attractors differed for each circuit. In fact, the new circuit generated symmetric trajectories. A detailed investigation proved that the chaotic responses in the proposed circuit could start at the peak-to-peak voltage of $V_f = 1.35$ V, at frequency 40 kHz, which was nearly half of the frequency value found for the ordinary circuit. Besides, a wide range of chaotic behavior was observed beyond $V_f = 0.675$ V and $f = 200$ kHz. Chaotic trajectories dominated the dynamics up to $f = 500$ kHz.

© 2014 Sharif University of Technology. All rights reserved.

1. Introduction

Nonlinear circuits have attracted wide interest due to their many applications in engineering [1-8]. While main objectives focus on encryption, signal masking and synchronization studies, important efforts for understanding chaos phenomena can also be mentioned [5-12]. Following the invention of chaos in a

basic circuit of the RL -diode by Lindsay [13], many theoretical and experimental studies have been undertaken in order to shed a light on the chaotic features of such a basic circuit and potential applications in secure communications and encryption [14-17]. Historically, the initial observations of Lindsay [13] and Testa et al. [14] have proven that periodic steady state behavior, with the same period as the voltage source, occurs as long as the source amplitude, V_f , is sufficiently small. However, if a certain feeding value of V_f is adjusted to the circuit input, the actual period of the steady state doubles. Thus, for V_f values which are just above

*. Corresponding author. Tel.: +90 312 202 8550;
Fax: +90 312 202 8550
E-mail address: ekurt52tr@yahoo.com (E. Kurt)

critical voltage, the output voltage over the resistor shows an 1/2 subharmonic, so called “bifurcation”. When V_f is further increased, an entire sequence of period-doubling bifurcations can be observed, such as 1/4, 1/8, 1/16 subharmonics. At the end of continuous bifurcations, the previous steady state can no longer be observed. Strictly speaking, the output signals are chaotic, except for some small transient periodic windows. Note that odd subharmonics were also observed for increasing voltages [13,14].

Azzouz et al. made a theoretical survey on the same circuit in order to identify the subharmonic features of the outputs [15]. They modeled the diode as a varactor diode and observed even and odd subharmonics. They also underlined the effect of nonlinear diode capacitances of the diodes rather than the effect of sharp delay [15]. Other studies undertaken into this nonlinear circuitry have focused on the route to chaos, which includes successive bifurcations just before the chaotic regime [18-21]. Many research papers have considered the determination of the so-called Feigenbaum parameters, which explains the universal recurrence relation of the trajectories in the bifurcating regime [16-19]. It has been proven that the bifurcation diagram obtained from the *RL*-diode circuit exhibits an ideal cycle with the Feigenbaum parameter, $\delta=4.669$ [14]. The *RL*-diode circuit has been used, not only for determination of bifurcation, but also for intermittency and quasi-periodicity [17-21]. From the point of time series analysis, there exist remarkable studies on the output voltages of the *RL*-Diode (*RLD*) circuit. For instance, one author of this paper explored the nonlinear responses of the *RLD* circuit via a statistical test by introducing an embedding dimension and applying it to the output [20,21]. Thereby, a nonlinear classification of the output signals was realized in a statistical manner. Although different orientations of *RL*-diode circuits have been studied in recent years [22,23], there are no studies on the effects of forward and reversed biased diode systems. In addition the analytical mechanism which causes a bifurcation in a diode current on the route to chaos, after successive period doublings, has not been studied before in such a circuit. It has been understood that the frequency of input signal and the resistor play an important role in defining the bifurcation point of the system, as in earlier findings in traditional *RLD* circuits [13,15,22,23]. The findings from the proposed circuit can be used in chaos synchronization circuits and jerk circuits, which can find many engineering applications in control and communication [6-8,24,25].

In the present paper, a new *RLD* circuit, namely *R-2L-2D*, is proposed, and a comparison between the dynamic responses of the ordinary and proposed circuits is presented. The proposed circuit has two diodes operating inversely, and two inductors. This

study is novel, since no studies exist in the literature on such connected circuit elements. The forward and reverse directed connections of the diodes and their effects on the phase space have not been discussed before. In addition, the proposed circuit exhibits a wider chaotic region compared to the traditional *R-L-D* circuit. The new circuit has a wider chaotic region, from $f=40$ kHz to 500 kHz in the parameter space, when the appropriate voltage amplitude is adjusted to the circuit.

The paper is organized as follows: Section 2 briefly describes the theoretical background of the proposed circuit. The equilibrium properties and bifurcation analysis are also handled in this section. The experimental details are presented in section 3. The main results and discussions are given in the next section. Finally, the paper ends with a brief conclusion on the main findings.

2. Theory of the proposed *R-2L-2D* circuit

The traditional *RLD* circuit, which is shown in Figure 1 (a), can be modeled by the following equations:

$$V_D + V_L + V_R = V_f,$$

$$I_D = I_0 \left[\exp \left(\frac{eV_D}{kT} \right) - 1 \right], \quad (1)$$

where V_f , V_D , V_L and V_R are the input voltage, and voltages across the diode, inductor and resistor, respectively. For such a model, period doubling can be found by measuring the voltage drop across the diode, with respect to the frequency or amplitude of the input signal, V_f . While I_0 is the saturation current of the diode, the denominator of the exponential function gives the heat energy at the junction of the diode, which is always accepted as a constant value in theoretical studies. Since the proposed *R-2L-2D* circuit includes additional elements, shown in Figure 1(b), the formulation is modified to the following:

$$V_R + V_{LD} = V_f, \quad (2)$$

where V_{LD} denotes the voltage across the branches of the inductor and diode. Note that the diodes are inversely attached to the inductors and parallel to each other. While current I splits into I_1 and I_2 on each diode branch, different parts of the sinusoidal signal pass through different branches over the entire period of the input signal. Therefore, one reads as:

$$V_{LD} = V_{D1} + L \frac{dI_1}{dt}, \quad \text{and} \quad V_{LD} = V_{D2} - L \frac{dI_2}{dt}. \quad (3)$$

Considering Figure 1 and the equations above, one arrives at:

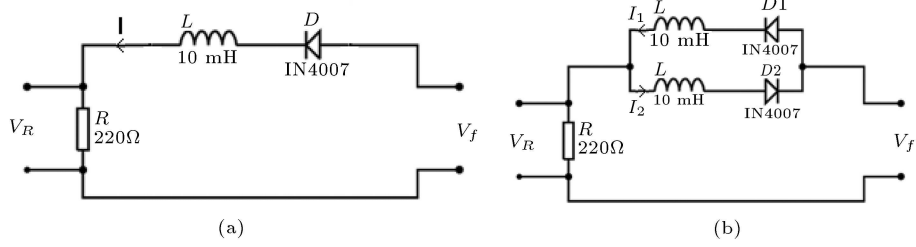


Figure 1. The circuit diagrams of the traditional R - L - D and the R - $2L$ - $2D$ circuits.

$$\begin{aligned} \frac{dI_1}{dt} &= \frac{V_{D1}}{L} + \frac{V_f}{L} \sin(\omega t) - \frac{R}{L}(I_1 + I_2), \\ \frac{dI_2}{dt} &= -\frac{V_{D2}}{L} + \frac{V_f}{L} \sin(\omega t) - \frac{R}{L}(I_1 + I_2). \end{aligned} \quad (4)$$

Here, I_1 and I_2 denote the branch currents, and $I = I_1 + I_2$ exists, and V_{D1} and V_{D2} are used for the voltages over the diodes. V_{D1} and V_{D2} are defined by the following functions:

$$\begin{aligned} V_{D1} &= \frac{kT}{e} \ln \left(\frac{I_1}{I_s} + 1 \right), \\ V_{D2} &= \frac{kT}{e} \ln \left(\frac{I_2}{I_s} + 1 \right). \end{aligned} \quad (5)$$

So that the nonlinear features of the diodes come into play when currents flow through them in forward directions. Note that this equation is also valid for backward directions, since it includes a saturation current term, denoted by I_s . This term is $I_s = 2.55 \text{nA}$ on average for the 1N4007 diode, which has been used in our experiments [26].

Considering the dimensionless forms of the above expressions, one arrives at:

$$\begin{aligned} \frac{dI_1}{dt'} &= \frac{kT}{eL} \ln \left(\frac{I_1}{I_s} + 1 \right) + \frac{V_f}{L} \sin(\Omega t') - \frac{R}{L}(I_1 + I_2), \\ \frac{dI_2}{dt'} &= -\frac{kT}{eL} \ln \left(\frac{I_2}{I_s} + 1 \right) + \frac{V_f}{L} \sin(\Omega t') - \frac{R}{L}(I_1 + I_2). \end{aligned} \quad (6)$$

In order to provide a dimensionless set of equations for analytical and numerical studies, one requires new definitions for variables. Therefore, time scaling $t' = \tau t$ can be considered, and τ is determined by the circuit element characteristics, such as $\tau = L/R$. Without using such a time scaling process, the equations cannot be analyzed parametrically, since the dimensionless parameters can either become too small or too large. Note that τ is nothing else than the natural period of the circuit and is not related to the period of externally applied voltage (i.e. $2\pi/\omega$). By simplifying the above

equations, one reads as:

$$\begin{aligned} \frac{dI_1}{dt} &= \alpha \ln \left(\frac{I_1}{I_s} + 1 \right) + \beta \sin(\omega t) - (I_1 + I_2), \\ \frac{dI_2}{dt} &= -\alpha \ln \left(\frac{I_2}{I_s} + 1 \right) + \beta \sin(\omega t) - (I_1 + I_2). \end{aligned} \quad (7)$$

The resulting system of equations can be written as follows:

$$\begin{aligned} \dot{x} &= \alpha \ln(x + 1) + \beta \sin(z) - (x + y), \\ \dot{y} &= -\alpha \ln(y + 1) + \beta \sin(z) - (x + y), \\ \dot{z} &= \Omega \frac{L}{R}. \end{aligned} \quad (8)$$

The third equation in Eq. (8) determines the main experimental parameter-frequency of the external signal. Note that x and y denote currents I_n and the relations $x = I_1/I_s$ and $y = I_2/I_s$ exist. The feeding frequency of the exciting voltage source is determined as a first-order variable, z . In addition, the parameters read as:

$$\alpha = \frac{kT}{eI_s R}, \quad \text{and} \quad \beta = \frac{V_f}{R I_s}. \quad (9)$$

Here, while α denotes the inverse of the resistance, β mostly characterizes the feeding voltage.

2.1. Equilibrium properties and bifurcation analysis

In this section, an analytical analysis of the three-dimensional continuous system given by Eq. (8) will be presented. The solution of the equilibrium points can be realized as follows:

$$\begin{aligned} 0 &= \alpha \ln(x + 1) + \beta \sin(z) - (x + y), \\ 0 &= -\alpha \ln(y + 1) + \beta \sin(z) - (x + y), \\ 0 &= \Omega \frac{L}{R}. \end{aligned} \quad (10)$$

Here, the system variables are considered to satisfy $\dot{x} = 0$; $\dot{y} = 0$ and $\dot{z} = 0$, as usual. Then, the equilibrium point is found as $S_1(x, y, z) = (0, 0, 0)$.

One can define the Jacobean matrix at $S_1(0, 0, 0)$ in the form of:

$$J = \begin{vmatrix} \alpha - 1 & -1 & \beta \\ -1 & -\alpha - 1 & \beta \\ 0 & 0 & 0 \end{vmatrix}. \quad (11)$$

In order to describe the bifurcation scenario, one has to define a bifurcation parameter. In our case, β is considered the main bifurcation parameter, as in many previous studies, since it controls the input voltage of the circuit. Eigenvalues λ of Eq. (13) can be found as follows:

$$J = \begin{vmatrix} \alpha - 1 - \lambda & -1 & \beta \\ -1 & -\alpha - 1 - \lambda & \beta \\ 0 & 0 & -\lambda \end{vmatrix} = 0. \quad (12)$$

After the calculation of this determinant, one reads as:

$$\begin{aligned} \lambda_1 &= 0, \\ \lambda_2 &= -1 - \sqrt{1 + \alpha^2}, \\ \lambda_3 &= -1 + \sqrt{1 + \alpha^2}, \end{aligned} \quad (13)$$

for the eigenvalues. According to these eigenvalue sets, while the first two eigenvalues give zero and negative results, the third one becomes positive and drives the system to chaos, as will be shown in Figure 8 later. Note that the resistor is in α (i.e. $1/R$). Thereby, for very high resistances, α will diverge to zero and the system will then be regular again. In our case, it gives $\lambda_3 \approx 45000$, which is high enough from zero. Eq. (13) can be obtained as the root of the third order determinant expression from Eq. (12), as follows:

$$(\alpha - 1 - \lambda)\{(\alpha + 1 + \lambda) - \lambda\} = 0. \quad (14)$$

In order to carry out the bifurcation analysis on the equilibrium point S_1 , we need to find out the eigenvectors of Eq. (15). In addition, the bifurcation

parameter, $\beta = 0$, should be ascertained. Thus, we arrive at:

$$\begin{aligned} (x_1, x_2, x_3) &= [0, 0, 1], \\ (x_1, x_2, x_3) &= [-\alpha + \sqrt{1 + \alpha^2}, 1, 0], \\ (x_1, x_2, x_3) &= [-\alpha - \sqrt{1 + \alpha^2}, 1, 0], \end{aligned} \quad (15)$$

for the corresponding eigenvectors. Then, one should transform the Jacobean matrix into its standard form. Using the eigenbasis of Eq. (15), the transformation matrix is defined as follows:

$$\begin{pmatrix} x \\ y \\ z \end{pmatrix} = \begin{pmatrix} 0 & -\alpha + \sqrt{1 + \alpha^2} & -\alpha - \sqrt{1 + \alpha^2} \\ 0 & 1 & 1 \\ 1 & 0 & 0 \end{pmatrix} \begin{pmatrix} x_1 \\ x_2 \\ x_3 \end{pmatrix}. \quad (16)$$

Eq. (9) is transformed into:

$$\begin{pmatrix} \cdot \\ x_1 \\ \cdot \\ x_2 \\ \cdot \\ x_3 \end{pmatrix} = \begin{pmatrix} 0 & 0 & 0 \\ 0 & -\frac{1-\alpha+\sqrt{1+\alpha^2}}{(2\sqrt{1+\alpha^2})^2} & \frac{\alpha}{(\sqrt{1+\alpha^2})^2} \\ 0 & \frac{\alpha}{(\sqrt{1+\alpha^2})^2} & -\frac{(-1+\alpha+\sqrt{1+\alpha^2})^2}{(2\sqrt{1+\alpha^2})^2} \end{pmatrix} \times \begin{pmatrix} x_1 \\ x_2 \\ x_3 \end{pmatrix} + \begin{pmatrix} g_1 \\ g_2 \\ g_3 \end{pmatrix}, \quad (17)$$

by use of the transformation matrix. Here, g_1, g_2 and g_3 are defined in Eq. (18) shown in Box I. Since the definitions, g , include all system dimensions, the stability of the equilibrium point, S_1 , near $\beta = 0$, should be examined. From the point of the central manifold theory, the stability of the equilibrium points (i.e. S_1) at the vicinity of $\beta = 0$ can be found by applying a one-parameter family of first-order ordinary differential equations on a center manifold. Therefore, we define:

$$\begin{aligned} x_2 &= h_1(x_1, \beta) = \alpha_1 x_1^2 + \alpha_2 x_1 \beta + \alpha_3 \beta^2 + h.o.t, \\ x_2 &= h_2(x_1, \beta) = b_1 x_1^2 + b_2 x_1 \beta + b_3 \beta^2 + h.o.t, \end{aligned} \quad (19)$$

$$\begin{aligned} g_1 &= \frac{\Omega L}{R^2 \sqrt{1 + \alpha^2}}, \\ g_2 &= \frac{-\alpha(\ln(1+x_2+x_3) + (\alpha - \sqrt{1 + \alpha^2}) \ln(1+x_2(-\alpha + \sqrt{1 + \alpha^2}) - x_3(\alpha + \sqrt{1 + \alpha^2}))) + \beta(1 - \alpha + \sqrt{1 + \alpha^2}) \sin x_1}{2\sqrt{1 + \alpha^2}}, \\ g_3 &= \frac{-\alpha(\ln(1+x_2+x_3) + (\alpha - \sqrt{1 + \alpha^2}) \ln(1+x_2(-\alpha + \sqrt{1 + \alpha^2}) - x_3(\alpha + \sqrt{1 + \alpha^2}))) - \beta(-1 + \alpha + \sqrt{1 + \alpha^2}) \sin x_1}{2\sqrt{1 + \alpha^2}}. \end{aligned} \quad (18)$$

Box I

in order to find out the vector field on the center manifold. According to the definition of the center manifold theory, one can find out a graph over the x_3 and β bifurcation parameter, as follows:

$$\begin{aligned} W_c(0) = & \{(x_2, x_2, x_3, \beta) \in R^4 | x_1 \\ & = h_1(x_1, \beta), x_2 \\ & = h_2(x_1, \beta), |x_1| < \delta, |\beta| \\ & < \bar{\delta}, h_i(0, 0) = 0, i = 2, 3\}, \end{aligned} \quad (20)$$

for δ and $\bar{\delta}$ which are small sufficiently. From the study of Wiggins [27], such a center manifold must satisfy the statement:

$$N(h(x, \beta)) = Dh0g_1 - Bh - g = 0, \quad (21)$$

where:

$$h = \begin{bmatrix} h_1 \\ h_2 \end{bmatrix}, \quad g = \begin{bmatrix} g_2 \\ g_3 \end{bmatrix}, \quad \text{and}$$

$$B = \begin{bmatrix} -\frac{(1-\alpha+\sqrt{1+\alpha^2})^2}{(2\sqrt{1+\alpha^2})} & \frac{\alpha}{(\sqrt{1+\alpha^2})} \\ \frac{\alpha}{(\sqrt{1+\alpha^2})} & -\frac{(-1+\alpha+\sqrt{1+\alpha^2})^2}{(2\sqrt{1+\alpha^2})} \end{bmatrix}. \quad (22)$$

Substituting Eqs. (19) into Eq. (21) and using h, g and B in Eq. (22), we get the terms with $x_1, x_1^2, x_1\beta, \beta^2$ and relevant constants from the expression below:

$$\begin{bmatrix} \cdot \\ h_1 \\ \cdot \\ h_2 \end{bmatrix} \cdot g_1 - \begin{bmatrix} -\frac{(1-\alpha+\sqrt{1+\alpha^2})^2}{(2\sqrt{1+\alpha^2})} & \frac{\alpha}{(\sqrt{1+\alpha^2})} \\ \frac{\alpha}{(\sqrt{1+\alpha^2})} & -\frac{(-1+\alpha+\sqrt{1+\alpha^2})^2}{(2\sqrt{1+\alpha^2})} \end{bmatrix} \cdot \begin{bmatrix} h_1 \\ h_2 \end{bmatrix} - \begin{bmatrix} g_2 \\ g_3 \end{bmatrix} = 0. \quad (23)$$

Following expressions for the constants from the above equation, one gets:

$$\begin{aligned} x_1 : a_1 \frac{\Omega L}{R\sqrt{1+\alpha^2}} &= 0; \rightarrow a_1 = 0, \\ x_1^2 : \left(\frac{\alpha}{2\sqrt{1+\alpha^2}} + \frac{(1-\alpha+\sqrt{1+\alpha^2})}{2\sqrt{1+\alpha^2}} \right) & \\ - \frac{(-\alpha^2+\alpha\sqrt{1+\alpha^2})(-\alpha+\sqrt{1+\alpha^2})}{2\sqrt{1+\alpha^2}} \right) a_1 & \\ = 0; \rightarrow a_1 = 0, & \end{aligned}$$

$$\begin{aligned} x_1\beta : a_2 : & \left(\frac{(1-\alpha+\sqrt{1+\alpha^2})^2}{2\sqrt{1+\alpha^2}} \right. \\ & \left. - \frac{(-\alpha^2+\alpha\sqrt{1+\alpha^2})(-\alpha+\sqrt{1+\alpha^2})}{2\sqrt{1+\alpha^2}} \right. \\ & \left. - \frac{\alpha}{2\sqrt{1+\alpha^2}} \right) - \frac{1-\alpha+\sqrt{1+\alpha^2}}{2\sqrt{1+\alpha^2}} = 0; \\ \rightarrow a_2 = & \frac{1}{1+\alpha^2+\sqrt{1+\alpha^2}-\alpha\sqrt{1+\alpha^2}}, \\ \beta^2 : & \left(\frac{(1-\alpha+\sqrt{1+\alpha^2})^2}{2\sqrt{1+\alpha^2}} + \frac{\alpha}{2\sqrt{1+\alpha^2}} \right. \\ & \left. - \frac{(-\alpha^2+\alpha\sqrt{1+\alpha^2})(-\alpha+\sqrt{1+\alpha^2})}{2\sqrt{1+\alpha^2}} \right) \\ \times a_3 = 0; \rightarrow a_3 = 0. \\ x_1 : b_1 \frac{\Omega L}{R\sqrt{1+\alpha^2}} &= 0; \rightarrow b_1 = 0 \\ x_1^2 : & \left(\frac{\alpha}{2\sqrt{1+\alpha^2}} + \frac{(\alpha-1+\sqrt{1+\alpha^2})^2}{2\sqrt{1+\alpha^2}} \right. \\ & \left. - \frac{(2\alpha^3+2\alpha^2\sqrt{1+\alpha^2}+\alpha)}{2\sqrt{1+\alpha^2}} \right) b_1 \\ = 0; \rightarrow b_1 = 0, & \\ x_1\beta : b_2 : & \left(\frac{(\alpha-1+\sqrt{1+\alpha^2})^2}{2\sqrt{1+\alpha^2}} \right. \\ & \left. - \frac{(2\alpha^3+2\alpha^2\sqrt{1+\alpha^2}+\alpha)}{2\sqrt{1+\alpha^2}} \right) \\ + \frac{\alpha}{2\sqrt{1+\alpha^2}} \right) - \frac{\alpha-1+\sqrt{1+\alpha^2}}{2\sqrt{1+\alpha^2}} = 0; \rightarrow b_2 = \\ \frac{1-\alpha-\sqrt{1+\alpha^2}}{2(-1+\alpha+\alpha^3+\sqrt{1+\alpha^2}-\alpha\sqrt{1+\alpha^2}+\alpha^2(-1+\sqrt{1+\alpha^2}))}, & \\ \beta^2 : & \left(\frac{(\alpha-1+\sqrt{1+\alpha^2})^2}{2\sqrt{1+\alpha^2}} + \frac{\alpha}{2\sqrt{1+\alpha^2}} \right. \\ & \left. - \frac{(2\alpha^2+2\alpha^2\sqrt{1+\alpha^2}+\alpha)}{2\sqrt{1+\alpha^2}} \right) \\ b_3 = 0; \rightarrow b_3 = 0. & \end{aligned} \quad (24)$$

Then, we obtain the definitions below for h_1, h_2 and h_3 :

$$\begin{aligned} x_2 &= h_1(x_1, \beta) = a_2 x_1 \beta + \dots \\ x_3 &= h_2(x_1, \beta) = b_2 x_1 \beta + \dots \end{aligned} \quad (25)$$

Consequently, if one substitutes the above expressions into Eqs. (19) and (17), the vector field reduced to the centre manifold is obtained as follows:

$$\begin{aligned} x_1 &= \frac{\Omega L}{R^2 \sqrt{1 + \alpha^2}}, \\ \dot{x}_1 &= 0. \end{aligned} \quad (26)$$

This result proves that the feeding frequency of the circuit plays an important role in understanding the bifurcation branches for the amplitude of feeding voltage.

3. Experimental

A schematic diagram of our experimental setup is shown in Figure 1 for the new circuit. For the ordinary *RLD* circuit, the setup is easy to apply, as in the literature. For both circuits, the circuit elements are defined as the resistances, $R = 220\Omega$, and the inductors, $L = 10mH$. In the case of diodes, the diodes are selected as 1N4007. The circuit is driven by a *BK Precision 4017* function generator giving a sinusoidal feeding with an adjustable frequency, f , and an amplitude, V_f . For the circuit measurements and phase space observations, a Kenwood CS-4125 oscilloscope has been used.

According to the circuit structure of the proposed circuit, the diodes operate parallel to each other. In that case, while current passes through one of the diodes in one direction, the other diode does not allow the current. However, the current always flows through one of the diodes for any frequency range. This reality causes a finite voltage on the resistance, R , for the entire period of the circuit. Meanwhile, the period doubling mechanism comes into play in two directions when suitable frequencies are applied to the circuit input.

Throughout the study, the parameter space (i.e. the plane of $V_f - f$) has been explored in order to see the entire responses of two circuits. At a constant input voltage, the maximum potential over a diode is observed when the driving frequency is the same as the resonant one. During the parameter scan, a number of period doubling behaviors have also been observed as usual for both circuits. While the voltage increment step is 0.45 V for the *RLD* circuit, it is 0.225 V for the *R-2L-2D* circuit, in order to get much clearer results from the latter. In the entire study, the frequency increment step is adjusted as 10 kHz for lower frequency regions and 20 kHz for higher frequency regions. Thus, the frequency and input voltage ranges

of $f = 1$ kHz – 560 kHz and $V_f = 0V - 3.15V$ (for *RLD* circuit), $V_f = 0V - 1.575V$ (for *R-2L-2D* circuit) have been scanned by the step of $\Delta f = 20$ Hz and $\Delta V = 0.05V$, respectively.

4. Results and discussions

According to the experimental explorations, both circuits generate different types of attractors, from periodic to chaotic, depending on the input signal. Initially, we focus on the periodic attractors at low and high frequencies, respectively. Figures 2 and 3 show representative periodic attractors.

While the periodic attractors from the *R-2L-2D* circuit (left plots in Figures 2 and 3) have a symmetric trajectory, with respect to the center of the attractor, at relatively low frequencies (see the left plot in Figure 2), this symmetry changes to another symmetric appearance at high frequencies, as shown in the left plot in Figure 3. Strictly speaking, in the latter case, symmetry can be found, with respect to an almost vertical plane, which cuts the trajectories at the middle of the attractor (see the left plot in Figure 3). Note that two zigzag regions occur on the one-period (1P) attractor (Figure 2 (left)). On the other hand, the attractors from the ordinary *RLD* circuit differ from the ones from the *R-2L-2D* circuit by the lack of any



Figure 2. Periodic attractors from *R-2L-2D* (left) and *RLD* (right) circuits. Here and in the following attractor figures, horizontal axis is the input voltage whereas the vertical one is voltage across resistance V_R . $V_f = 0.9$ V for both plots and $f = 7.66$ kHz (left) and 3.2 kHz (right).

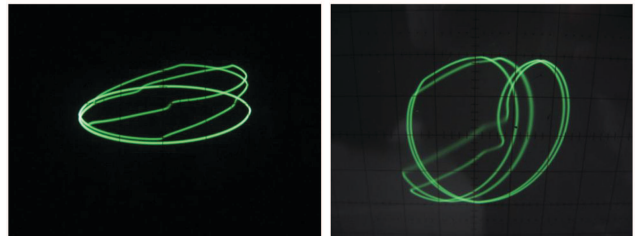


Figure 3. Periodic attractors with high harmonics: Three periodic regimes (3P) for *R-2L-2D* circuit (left) and four periodic regime (4P) for *RLD* circuit (right). $V_f = 0.9$ V for both plots and $f = 133.5$ kHz (left) and 85.7 kHz (right).

symmetric trajectories (see the right plots in Figures 2 and 3).

From the literature [13,14], it is known that the *RLD* circuit generates an asymmetric periodic attractor, as in our experiment. However, inversely-directed diodes cause a symmetrical appearance in the attractors from the *R-2L-2D* circuit. It is obvious that the voltage over resistor R takes different values for any values of input voltage.

A chaotic attractor having symmetry on the vertical plane passing through the center of the phase space is shown in Figure 4. This attractor appears when the frequency of the input signal is increased slightly from 133.5 kHz to 139.1 kHz.

Note that the overall shapes of trajectories resemble the case in Figure 3 (left). However, complicated trajectories complete the phase space representation. A representative chaotic attractor from the *RLD* circuit is shown in the right plot of Figure 4 at $f = 88.7$ kHz. The trajectories carry the general form shown in the right plot of Figure 4, especially, the trajectories in the middle of the attractor are clearly seen having a growing distance from each other.

In the lower frequency regime of the *R-2L-2D* circuit, one can also see even periodic (i.e. period four 4P) behavior, as shown in the left plot of Figure 5. It is known from the literature that both successive even and odd periodic transitions can occur, depending on the frequency [14]. Therefore either odd periodic transitions (shown in the left plot of Figure 3) or

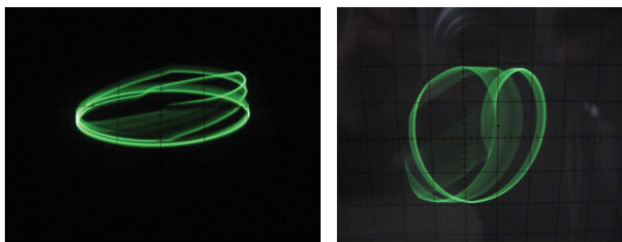


Figure 4. Chaotic attractors from *R-2L-2D* (left) and *RLD* (right) circuits at relatively high frequencies. $V_f = 0.9$ V for both plots and $f = 139.1$ kHz (left) and 88.7 kHz (right).

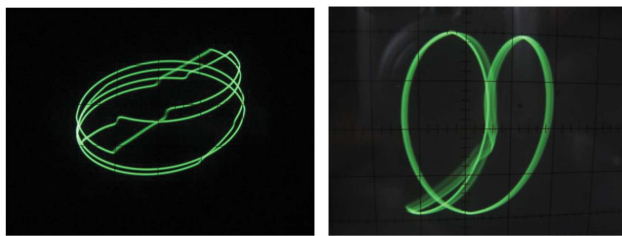


Figure 5. A 4P periodic (left) and quasi-periodic (right) attractors from *R-2L-2D* and *RLD* circuits, respectively. $V_f = 0.9$ V for both plots and $f = 76.5$ kHz (left) and 107.6 kHz (right).

even periodic ones can be observed in the new circuit. Note also that the main appearance of the attractor is preserved for all subharmonic cases. In the right plot of Figure 5, a quasi-periodic regime is indicated for relatively high frequency in the *RLD* circuit. After the compilation of the periodic window, the circuit is driven to another chaotic attractor, which differs from the earlier one in Figure 4 (right).

When one increases the frequency further in the higher frequency chaotic regime, the attractor which is shown in Figure 4 is transformed into a complicated form, as given in Figure 6. Note that the individual trajectories in the left plot of Figure 4 cannot be observed in the latter case, while the symmetrical appearance, with respect to the vertical plane, persists. However, the chaotic attractor obtained from the *RLD* circuit does not have the symmetry as in the earlier cases. An interesting chaotic attractor, which is obtained at a relatively lower frequency regime, from the *R-2L-2D* circuit, is shown in Figure 7. Note that this attractor appears at $f = 71.4$ kHz, which is slightly lower frequency, as the case in Figure 5. The main difference between two chaotic regimes is that the chaotic trajectories become much more complicated, by coming near each other at a high frequency regime, than usual. While the individual trajectories can be selected to some extent at lower frequencies, this feature disappears at high frequencies, as in the left

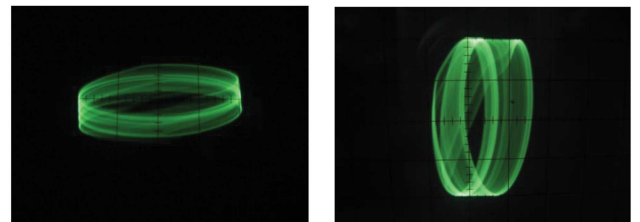


Figure 6. Chaotic attractors from *R-2L-2D* (left) and *RLD* (right) at high frequencies $f = 158.8$ kHz (left) and 194.1 kHz (right). $V_f = 0.9$ V for both plots.



Figure 7. A chaotic attractor at low frequency regime from *R-2L-2D* circuit: $(V_f, f) = (0.9V, 71.4$ kHz).

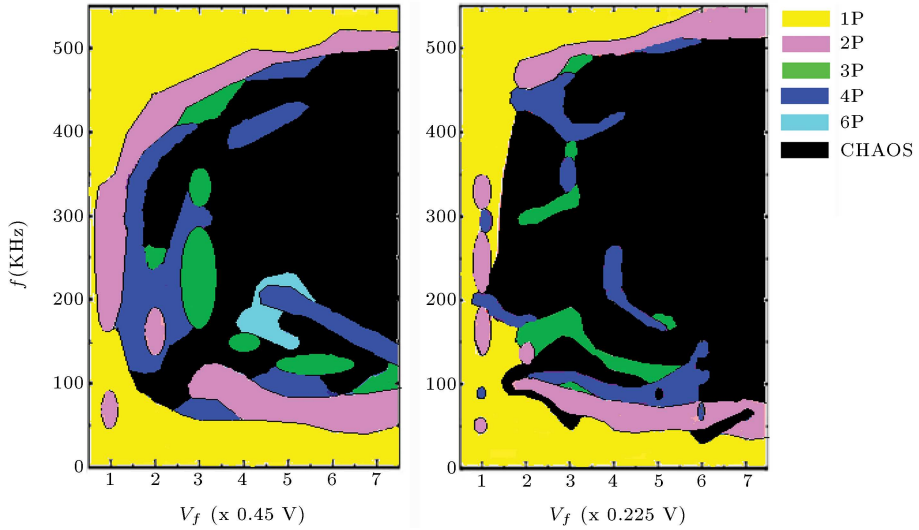


Figure 8. The experimental two-parameter bifurcation diagram as functions of feeding voltage (V_f) and frequency (f) for *RLD* (left) and *R-2L-2D* (right) circuits. The colors indicate the relevant dynamic reply of the circuits and can be seen better in electronic version of the paper.

plot of Figure 6. The symmetry in the trajectories can also be clearly seen in Figure 7.

In order to determine the entire dynamic response in the parameter space (i.e. the input frequency f and voltage V_f), we produce a detailed two-parameter bifurcation diagram in Figure 8 for both circuits. Such diagrams can also be seen in earlier studies [3,23] for the determination of the dynamic behavior of the circuits. Since it contains two main system parameters (i.e. f and V_f of input signal), it gives an overall idea where the circuit exhibits periodic and chaotic responses. In this diagram, the dynamic behaviors of the circuits are indicated as separated regions, which underline the periodic and chaotic regions, after successive bifurcating points, for a wide range of input signals. Note that the voltage values in the horizontal axis of the diagram are peak to peak values, whereas the frequency is in kHz.

It is proven that the chaotic region indicated by black is enlarged down to relatively lower frequencies in the proposed circuit compared to the traditional *RLD* circuit. In addition, there exist large regions, where the current flowing through the main branch goes to chaos directly from the 1P region. In a most recent study, Manimehan and Philominathan [23] also observed such regions in their own circuitry, when they considered parallel-attached elements. It is also interesting that the occurrence of chaotic regions in their study [23] and the present one follows a similar rule, such as $V_f \approx (f - f_0)^2 + a$. Here, f_0 denotes the frequency value, where the minimal V_f sits, and a is a constant, which carries the parabola upwards from the frequency axis. In order to determine the exact function, a fitting curve can be drawn for further studies. However, it is beyond the present paper. While the yellow color represents 1P

output, the chaotic behavior is denoted by black. Note that some higher periodic bifurcations can also be seen adjacent to the chaotic region in general. In addition, the proposed circuit can generate chaotic responses for relatively low voltage and frequency values compared to the *RLD* circuit. From the point of frequency, the upper boundary for the chaotic responses does not change too much compared to the findings from the *RLD* circuit. There exist multiple chaotic regimes among the several periodic windows including the successive period doubling mechanism. Note, also, that odd and even subharmonic behaviors are observed in both circuits clearly, as also observed in previous studies [14,15].

While the first chaotic response has been obtained at $(V_f, f) = (1.35 \text{ V}, 40 \text{ kHz})$ at a low frequency regime, the parameter set $(V_f, f) = (0.225 \text{ V}, 160 \text{ kHz})$ also gives a chaotic response at a low voltage region. In addition, a wide region of chaos persists between the values, $(V_f, f) = (1.125 - 1.575 \text{ V}, 200 - 400 \text{ kHz})$, for the scanned parameter region. We believe that these chaotic responses can also dominate the dynamics for much higher amplitudes. Thereby, this circuitry can efficiently serve to generate chaotic signals for a large range of parameters.

5. Conclusions

A new circuit, namely *R-2L-2D*, with double inductors and diodes, is introduced, and the dynamic responses are discussed compared with the ordinary *RLD* circuit using the same circuit elements. It has been found that this new circuitry reflects the characteristics of the *RLD* circuit from the point of successive bifurcation regimes and multiple chaotic regimes, with respect to

the input voltage and frequency. This study is novel in the sense that the literature does not contain any information in regard to the proposed circuit with the forward and reverse directed connection of the diodes. This kind of connection yields to many symmetrical attractors. In addition, the proposed circuit exhibits a wider chaotic region compared to the traditional *R-L-D* circuit. Strictly speaking, the attractors observed in the *R-2L-2D* circuit have certain symmetries, according to either the center of the attractor or the vertical plane passing through the center of the phase space apart from the ordinary *RLD* circuit. In addition, the trajectories become much complicated for high frequency inputs for both circuits. It can be also concluded that the chaotic region enlarges toward the lower frequencies in the proposed circuit, whereas the dynamics resemble ordinary *RLD* circuits at higher frequencies. In addition, new circuitry can generate the chaotic dynamics at lower voltages compared to the *RLD* circuit. Therefore we expect that this new circuit can easily serve the fundamental theory of chaos and bifurcation, since the dependence on the excitation frequency determines the bifurcation scenario for a constant excitation voltage. Due to its simple circuitry, the proposed circuit can also be used for the educational purposes of engineers and physicists in the labs.

References

1. Kurt, E. and Cantürk, M. "Bifurcations and hyperchaos from a dc driven non-identical Josephson junction system", *Int. J. Bif. Chaos*, **20**(11), pp. 3725-3740 (2010).
2. Kurt, E. and Cantürk, M. "Chaotic dynamics of resistively coupled DC-driven distinct Josephson junctions and the effects of circuit parameters", *Physica D: Nonl. Phen.*, **238**(22), pp. 2229-2237 (2009).
3. Kurt, E. "Nonlinearities a non-autonomous chaotic circuit with a non-autonomous model of Chua's diode", *Phys. Scr.*, **74**, pp. 22-27 (2006).
4. Kurt, E., Ozturk, M.K. and Kasap, R. "Investigating the most appropriate parameters of the nonlinear resistor circuit time series", *J. Inst. Sci. & Tech. Gazi Uni.*, **14**(4), pp. 1261-1269 (2001).
5. Thompson, J.M.T. and Bishop, S.R., *Nonlinearity and Chaos in Engineering Dynamics*, John Wiley and Sons, England (1994).
6. Kennedy, M.P., Rovatti, R. and Setti, G. (edited by Raton, B.), *Chaotic Electronics in Telecommunications*, CRC Press, FL (2000).
7. Uchida, A., Davis, P. and Itaya, S. "Generation of information theoretic secure keys using a chaotic semiconductor laser", *Appl. Phys. Lett.*, **83**(15), pp. 3213-3215 (2003).
8. Van Wijgeren, G.D. and Roy, R. "Communication with chaotic lasers", *Science*, **279**, pp. 1198-1200 (1998).
9. Dana, S.K., Sengupta, D. and Edoh, K. "Chaotic dynamics in Josephson junction", *IEEE Trans. Circuits Systems I: Fund. Theory and Appl.*, **48**(8), pp. 990-996 (2001).
10. Kapitaniak, T., *Controlling Chaos*, Academic Press, San Diego (1996).
11. Stojanovski, T., Pihl, J. and Kocarev, L. "Chaos based random number generators - Part II: Practical realization", *IEEE Trans. Circ. Syst.-I: Fund. Theo. Appl.*, **48**, pp. 382-385 (2001).
12. Tsubone, T. and Saito, T. "Hyperchaos from a 4-D manifold piecewise-linear system," *IEEE Trans. Circ. Syst.-I: Fund. Theo. Appl.*, **45**, pp. 889-894 (1998).
13. Lindsay, P.S. "Period doubling and chaotic behaviour in a driven anharmonic oscillator", *Phys. Rev. Lett.*, **47**, pp. 1349-1352 (1981).
14. Testa, J., Perez, J. and Jeffries, C. "Evidence for universal chaotic behaviour of a driven oscillator", *Phys. Rev. Lett.*, **48**, pp. 714-717 (1982).
15. Azzouz, A., Duhr, R. and Hasler, M. "Transition to chaos in a simple nonlinear circuit driven by a sinusoidal voltage source", *IEEE Trans. Circuits Syst., CAS-30* (1983).
16. Su, Z., Rollings, R.W. and Hunt, E.R. "Universal properties at the onset of chaos in diode resonator systems", *Phys. Rev. A*, **40**(5), pp. 2689-2697 (1989).
17. Van Buskirk, R. and Jeffries, C. "Observation of chaotic dynamics of coupled nonlinear oscillators", *Phys. Rev. A*, **31**, pp. 3332-3357 (1985).
18. Huang, J.Y. and Kim, J.J. "Type-II intermittency in a coupled nonlinear oscillator: Experimental observation", *Phys. Rev. A*, **36**(3), pp. 1495-1497 (1987).
19. Kim, Y.H. and Kim, J.J. "Observation of quasiperiodicity in a single diode circuit", *J. Korean Phys. Soc.*, **27**(2), pp. 225-227 (1994).
20. Kasap, R. and Kurt, E. "Investigation of chaos in the RL-diode circuit by using the BDS test", *J. Appl. Math. Decision Sci.*, **2**(2), pp. 193-199 (1998).
21. Kurt, E., Acar, S. and Kasap, R. "A comparison of chaotic circuits from a statistical approach", *Math. Comp. App. J.*, **5**(2), pp. 95-103 (2000).
22. Inaba, N., Nishio, Y. and Endo, T. "Chaos via torus breakdown from a four-dimensional autonomous oscillator with two diodes", *Physica D*, **240**(11), pp. 903-912 (2011).
23. Manimehan, I. and Philominathan, P. "Composite dynamical behaviors in a simple series-parallel LC circuit", *Chaos, Solitons and Fractals*, **45**(12), pp. 1501-1509 (2012).
24. Munmuangsaen, B., Srisuchinwong, B. and Sprott, J.C. "Generalization of the simplest autonomous chaotic system", *Physics Letters A*, **375**, pp. 1445-1450 (2011).

25. Sprott, J.C. "A new chaotic jerk circuit", *IEEE Trans. Circuits and Systems-II: Express Briefs*, **58**(4), pp. 240-243 (2011).
26. <http://www.buildinggadgets.com/1N4007.pdf>
27. Wiggins, S., *Introduction to applied nonlinear dynamical systems and chaos*, Springer-Verlag, New York (1990).

Biographies

Erol Kurt completed his undergraduate studies at Gazi University, Turkey, in 1998, and obtained his MS degree from the Institute of Science and Technology of the same university in 2001. He completed his PhD degree in 2004, at Bayreuth University, Germany. He is currently Professor in the Department of Electrical and Electronics Engineering at the Technology Faculty of Gazi University, Turkey. His main teaching and research areas include nonlinear phenomena in electrical/electronic circuits, electric machine design, mechanical vibrations, chaos, plasmas, fusion and magnetohydrodynamics. He has authored and co-authored many scientific papers and has been guest editor of several special issue journals. He is also Technical Chairman of the annual International Conference of Nuclear and Renewable Energy Resources (NuRER)

and Chairman of the European Conference and Workshop on Renewable Energy Systems (EWRES).

Bünyamin Ciylan was born in 1971 in Adana, Turkey. He obtained BS, MS and PhD (2009) degrees from the Department of Electronics and Computer Education at Gazi University, Turkey, where he is currently Assistant Professor. He is also Deputy Director of the Continuous Educational Center. His research interests include thermoelectric test systems, measuring systems and artificial neural networks.

Omer Oguz Taskan graduated in 2013 from the Department of Electrical Education at the Technical Education Faculty of Gazi University in Ankara, Turkey, where he is currently an MS degree student. His specialty is electrical circuits modelling.

Hatice Hilal Kurt received her BS, MS, and PhD degrees in 1997, 2000 and 2004, respectively, from Gazi University, Ankara, Turkey, where she is currently Associate Professor in the Department of Physics. Her research interests include gas discharges and high-speed infrared-visible conversion techniques in semiconducting plasma structures, as well as the electrical properties of semiconductor elements.